

The internal structure of single carbon fibers determined by simultaneous small- and wide-angle X-ray scattering

Oskar Paris^a, Dieter Loidl^b, Herwig Peterlik^b, Martin Müller^c, Helga Lichtenegger^a, and Peter Fratzl^a

^a *Erich Schmid Institute of Materials Science, Austrian Academy of Sciences, and Metal Physics Institute, University of Leoben, Jahnstrasse 12, A-8700 Leoben, Austria,* ^b*Institute of Materials Physics, University of Vienna, Boltzmannngasse 5, A-1090 Vienna, Austria,* and ^c*European Synchrotron Radiation Facility, B.P. 220, F-38043 Grenoble Cedex 9, France.*
E-mail: Paris@unileoben.ac.at

Simultaneous small-angle scattering and wide-angle diffraction using a synchrotron radiation microbeam was applied for the first time to investigate single carbon fibers in a position-resolved way. Taking into account the exact X-ray beam profile and examining the fibers in two scattering geometries allowed a discrimination between different models for the internal arrangement of carbon layers and pores. For a fiber based on polyacrylonitrile the carbon layers were randomly oriented within the fiber cross section, whereas in a mesophase-pitch based fiber the layers were arranged in a radial structure.

1. Introduction

Carbon fibers may be considered nano-composites, consisting of three components, quasi-amorphous and crystalline regions, and pores (Kobets & Deev, 1997). Many of the outstanding mechanical properties are attributed to the internal structure of the fibers, e.g., to a preferred orientation of carbon layers and to possible skin-core effects (Ruland, 1990, and references therein). In the past three decades, wide-angle X-ray diffraction (WAXD) was extensively used to determine the preferred orientation of the carbon layers as well as the size and shape of the crystalline regions (Ruland & Tompa, 1968; Perret & Ruland, 1970; Takaku & Shioya, 1990). From small-angle X-ray scattering (SAXS) experiments on fiber bundles it is known that long, thin pores are mainly oriented along the fiber axis, following the preferred orientation of the carbon layers (Perret & Ruland, 1969 & 1970; Gupta et al., 1994; Peterlik et al., 1994). In these studies, however, one was not able to resolve details of the structural arrangement within the fiber cross section. Information about the internal organization in single fibers was obtained by Scanning Electron Microscopy (Kobets & Deev, 1997) and Transmission Electron Microscopy (Bennett & Johnson, 1979), the latter technique allowing a direct, position-resolved observation of the arrangement of carbon layers using lattice-fringe imaging. In fibers based on polyacrylonitrile (PAN) a random arrangement of the carbon layers within the fiber cross section was usually observed, while for mesophase-pitch (MPP) based fibers the internal structure is known to depend strongly on the fiber production process. Pronounced non-random arrangements of the carbon layers within the fiber cross section, such as radial- or onion-skin structures, were reported for MPP-based fibers (Edie & Stoner, 1992).

In recent years, position-resolved X-ray scattering methods have been developed for the investigation of hierarchically structured materials (e.g. Fratzl et al., 1997). X-ray microbeams with sizes down to less than 1 μm have recently become available at synchrotron radiation sources, and thus, samples which are heterogeneous on a micrometer scale may be studied nowadays also in a position-resolved way using

X-ray microbeam scattering techniques (Riekkel et al., 1997; Müller et al., 1998; Lichtenegger et al., 1999). Here, we report first experiments revealing the internal structure of two different carbon fibers by means of simultaneous microbeam SAXS and WAXD. The aim of the present paper is to demonstrate that this technique allows one to discriminate between structural models for the internal organization of single carbon fibers.

2. Experimental

Two commercially available carbon fibers (PAN-based fiber *HTA7* from *Tenax GesmbH* and MPP-based fiber *FT500* from *Tonen*) were investigated. Both fibers were examined by Scanning Electron Microscopy (SEM), yielding circular fiber cross sections with diameters of 7.1 μm (*HTA7*) and 9.6 μm (*FT500*).

The scattering experiments were carried out at the microfocus beamline (ID13) at the European Synchrotron Radiation Facility (ESRF) in Grenoble, France. The monochromatic X-ray beam (wavelength $\lambda = 0.948 \text{ \AA}$) was focussed by an ellipsoidal mirror and a glass capillary (Riekkel et al. 1997). An area detector (MAR-CCD, active diameter 130 mm, pixel-size 64.5 $\mu\text{m} \times 64.5 \mu\text{m}$) was placed at a distance of 45 mm from the specimen and a small beam-stop (0.3 mm lead on a thin glass-fiber) was mounted at a distance of about 20 mm from the sample. This beam-stop position was found optimal for reduced air scattering (no evacuated beam path was available) as well as for reaching sufficiently small scattering angles. The setup allowed the simultaneous recording of SAXS and WAXD data with a single 2D-detector in the range of scattering vectors from $q = 0.1 \text{ \AA}^{-1}$ to 5 \AA^{-1} ($q = 4\pi \sin(\theta) / \lambda$, where 2θ is the scattering angle).

Since the size of the X-ray beam was only a factor 2 to 3 smaller than the diameter of the fibers, special effort was undertaken to determine the exact beam profile at the specimen position. This was done by scanning a circular pinhole (Pt-Ir, 20 μm diameter) in two orthogonal directions (y, z) perpendicular to the beam. The two-dimensional beam profile was derived by fitting a model function to both data sets, taking into account the curvature of the pinhole. The full width at half maximum (FWHM) of the beam at the sample position was determined to be 3.6 μm .

The samples could be scanned in the two directions y and z perpendicular to the beam with an accuracy of 0.1 μm , and the exact beam position with respect to the sample could be determined using an online video microscope. The fibers were examined in two different scattering geometries:

(i) the usual fiber geometry with the fiber axis perpendicular to the X-ray beam, and

(ii) a transverse geometry with the fiber axis parallel to the beam. For experiments in this geometry, a single fiber had to be embedded into resin, cut by a microtome to a length of about 3-5 μm and mounted on a copper grid. Linear scans were performed along two perpendicular directions of the fiber cross section for the PAN-based fiber *HTA7*. For the MPP-based fiber *FT500* a two-dimensional mesh-scan was carried out with a step size of 2 μm .

Typical measurement times were 30 s for a single scattering pattern. All measured data were normalized with respect to the primary beam monitor and corrected for background. Data evaluation was partly done using the software package *FIT2D* (Hammersley, 1999).

3. Results

Two different types of carbon fibers were investigated using synchrotron microbeam SAXS and WAXD. Fig. 1 shows examples of 2D scattering patterns taken in fiber geometry with the fiber axis being vertical (z -direction). On the equator (horizontal axis), the anisotropic SAXS signal near the incident beam indicates the

presence of elongated pores oriented mainly parallel to the fiber axis. Moreover, the 002 and 004 reflections from the parallel packing of the hexagonal carbon layers are visible. On the meridian (vertical axis) one identifies the 100 reflection (layer line) from the two-dimensional structure of the carbon layers.

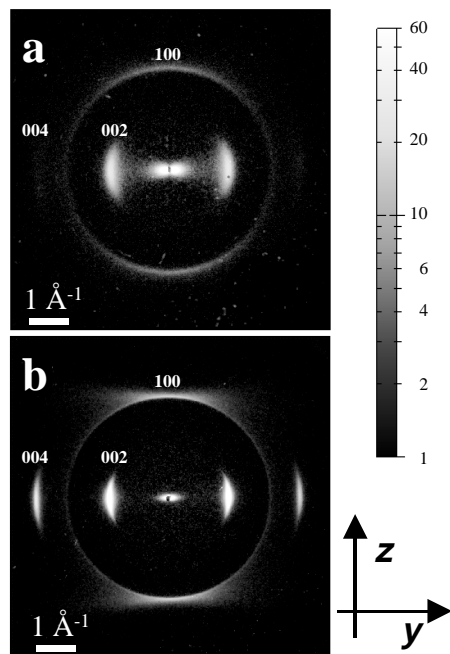


Figure 1

Two-dimensional scattering patterns obtained in fiber geometry at the center of (a) the PAN-based fiber *HTA7* and (b) the MPP-based fiber *FT500*. The wave vector transfer is given by the bars in the figures, and the reflections 100, 002 and 004 are indicated. The gray-level scale for the intensity at the right (in arbitrary units) is the same for both scattering patterns. Both patterns were normalized with respect to the primary beam monitor and to fiber thickness, so the gray-levels may be compared directly. The coordinate system on the lower right side defines the geometry of the scan experiment in real space: *z*-axis = fiber axis, *y*-axis = scan axis, *x*-axis (perpendicular to the paper plane) = beam axis.

There are remarkable differences in the two patterns, illustrating the variety of structural features in carbon fibers, depending on the type and heat-treatment (Ruland, 1990). This concerns in particular the widths of the intensity distributions, which are related to structural parameters like size, perfection and degree of orientation of the crystalline regions and size, shape and orientation of the pores. Similar patterns with the proper position resolution were up to now only obtained in electron diffraction studies (Fourdeux, Perret & Ruland, 1968; Bennett & Johnson, 1979). The main advantages of X-rays as compared with electrons include a better resolution in reciprocal space, no multiple scattering and a more quantitative evaluation of these scattering patterns. A detailed discussion of all the structural features is, however, beyond the scope of this paper. Similar patterns as in Fig. 1 were derived in fiber geometry as a function of position *y* by scanning the fibers perpendicular to the beam with steps of 0.5 μm. For a fully random arrangement of the carbon layers within the volume illuminated by the X-ray beam, the intensity of the equatorial reflections would be smeared

homogeneously in rings within the *x-y* plane in reciprocal space. In this case the measured scattering patterns in fiber geometry would show a change of the total intensity of the equatorial reflections proportional to the actual fiber volume illuminated by the X-ray beam. For any kind of preferred orientation of the carbon layers, however, a texture effect is expected which would affect the total intensity of the equatorial reflections. Therefore, the total intensity of the 002 reflection within the detector plane (denoted as I_{002}) was calculated, and is drawn in Figs. 2a and 2b as a function of position *y* for the fibers *HTA7* and *FT500*, respectively. In order to compare these data with the distribution expected for a random arrangement of carbon layers within the fiber cross section, we have calculated the convolution

$$\Omega(y) = f(y) \otimes d(y) \quad (1)$$

where $f(y)$ is the beam profile projected to the *y*-direction and

$$d(y) = 2\sqrt{R^2 - y^2} \quad (2)$$

is the thickness of the fiber as a function of *y* (R = fiber radius).

The function $\Omega(y)$ for the respective fibers is drawn in Figs. 2a and 2b by solid lines. For the PAN-based fiber *HTA7* (Fig. 2a), $\Omega(y)$ fits the experimental data quite well, in agreement with a random arrangement of the carbon layers. For the MPP-based fiber *FT500*, however, there is a considerable deviation of the calculated curve from the experimental data (Fig. 2d), indicating a non random orientation of the carbon layers within the cross section of this fiber.

It has already been demonstrated in a previous investigation on wood (Lichtenegger et al., 1999) that in a scattering geometry with the fiber axis parallel to the X-ray beam, it is possible to get more direct information about the internal structural organization within the fiber cross section. Fig. 3a shows a map of scattering patterns from a 2D mesh scan through the cross section of the MPP-based fiber *FT500* with the fiber axis oriented parallel to the beam. In the figure, scattering patterns were zoomed to visualize the SAXS signal only. The SAXS patterns near the center of the fiber are almost circular and

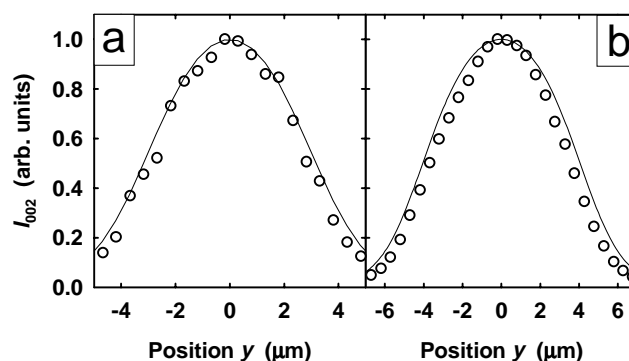


Figure 2

The total intensity of the 002 reflection is shown versus position *y* for the fibers (a) *HTA7* and (b) *FT500* by the open circles. The solid lines in (a) and (b) are the calculated values of Ω from equation (1), i.e., the convolution of the X-ray beam profile with the contour of the respective fiber (see text for details). The *y*-scale is different because of the different diameters of the two fibers (*HTA7*: $D_{\text{Fiber}} = 7.1 \mu\text{m}$, *FT500*: $D_{\text{Fiber}} = 9.6 \mu\text{m}$).

become elliptical outside, the short axes of the ellipses pointing consistently into radial fiber direction (Fig. 3*b*). The elliptical shape of the SAXS patterns is indicative of a non circular cross section of the pores. Note, that for a random distribution of pores the SAXS patterns would be circular symmetric at every position even for a non-circular pore cross section. Thus, taking a model of shelf-like pores (with their longest dimension along the fiber axis), the longer side of the pore cross section would point into radial fiber direction. Since shape and orientation of the pores must be connected with the arrangement of carbon layers, a radial arrangement of carbon layers within the fiber cross section is directly obvious from Fig. 3.

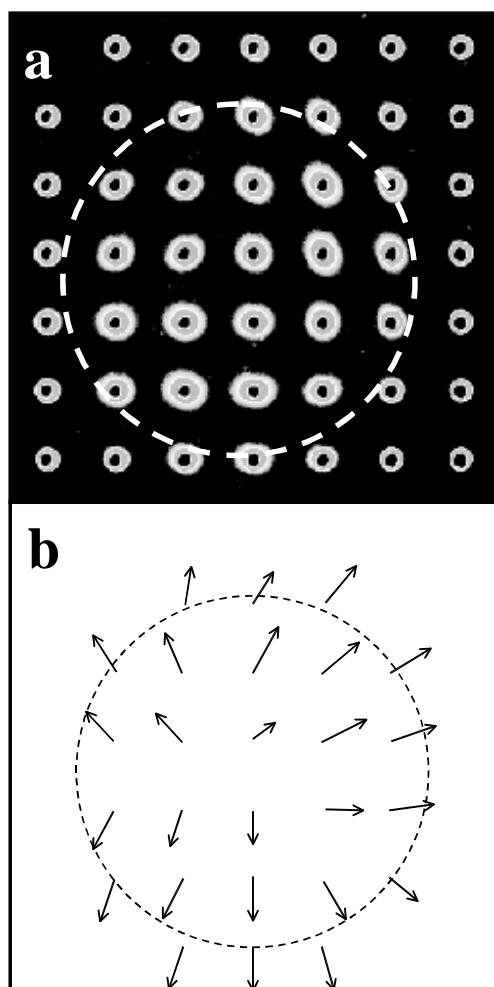


Figure 3

(*a*): Map of SAXS patterns combined according to a mesh scan over the cross section of the MPP-based fiber *FT500*. The fiber axis was parallel to the direction of the X-ray beam and the step size was 2 μm . Every "pixel" of the mesh scan corresponds to a single scattering pattern with a scattering vector range: $-0.3 \text{ \AA}^{-1} < q < 0.3 \text{ \AA}^{-1}$, horizontally and vertically. The dashed line indicates the border of the fiber. The signals outside the dashed line are mainly due to scattering contributions from the resin and from the guard pinhole. (*b*): The arrows indicate the direction of the short axis of the elliptical SAXS signal from (*a*). The length of the arrows is roughly proportional to the eccentricity of the ellipses.

The PAN-based fiber *HTA7* was also investigated in this geometry by performing linear scans along two perpendicular directions of the fiber cross section. In this case, the shape and orientation of the SAXS patterns did not change with position, indicating a random distribution of the pores and carbon layers within the fiber cross section.

4. Discussion

It is well documented in the literature (e.g. Ruland, 1990) that in PAN-based fibers the internal arrangement of carbon layers within the fiber cross section is random, while pronounced non-random structures are generally expected for MPP-based fibers. Consistent with the literature, the SAXS patterns obtained from the geometry with the fiber axis parallel to the beam indicate a radial arrangement of pores for the MPP-based fiber *FT500* (see Fig. 3), and a random distribution for the PAN-based fiber *HTA7*. For the measurements performed in standard fiber geometry, the orientation of carbon layers and pores is not directly visible in the scattering patterns. However, when compared with the total volume illuminated by the beam (as expressed by equation 1), the position dependence of I_{002} is consistent with a random structure only for *HTA7* (Fig. 2*a*). For *FT500* the experimental data deviate clearly from the curve expected for a random arrangement (Fig. 2*b*). Nevertheless, it would be quite important to obtain more detailed information also from standard fiber geometry experiments, since it provides the possibility to investigate the fibers in a non destructive way. *In-situ* tension experiments for instance, which would give new insights in the relationship between structure and mechanical properties of carbon fibers could only be performed in this geometry. In the following, we present a simple picture which qualitatively relates the information obtained from the fiber geometry experiments (Fig. 2) to different models for the arrangement of carbon layers within the fibers.

For a certain fiber volume illuminated by the X-ray beam, the Bragg condition for the 002 reflection is fulfilled only for those carbon layers which are tilted by an angle of θ with respect to the incident beam ($2\theta = \text{Bragg angle}$). The situation is sketched for an onion-skin and a radial arrangement in Fig. 4. Assuming a certain distribution of tilt angles of the carbon layers with respect to a main direction, only regions within the shaded areas in Fig. 4 would fulfill the Bragg condition. Thus, the total intensity of the 002 reflection for a certain position is proportional to the intersection of the X-ray beam with the shaded area. Qualitatively this would lead to a decrease of the intensity from the borders toward the center of the fiber for an onion-skin arrangement (Fig. 4, left), while for a radial distribution (Fig. 4, right), a vanishing signal at the borders and a strong increase toward the center of the fiber should appear. Obviously, the signal would not depend on position for a fully random structure. In order to compare these considerations with the experimental data shown in Fig. 2, we have chosen two model functions $M(y)$, representing qualitatively the expected trend of the 002 intensity for the case of the onion-skin and the radial model. These two functions are shown in Figs. 5*a* and 5*b* for the fibers *HTA7* and *FT500*, respectively.

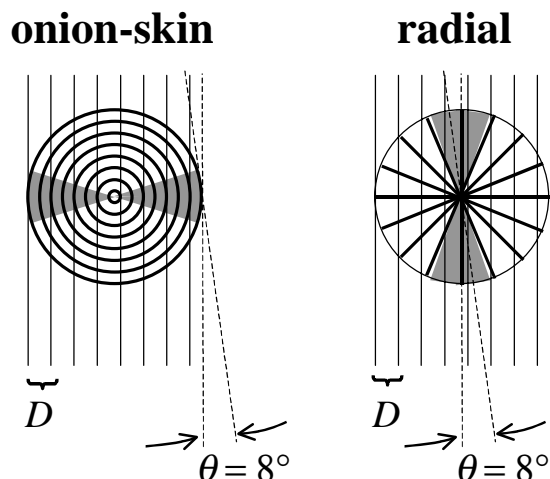


Figure 4

Sketch of the geometrical constraints for the Bragg condition of the 002 equatorial reflection ($2\theta = 16^\circ$) in fiber geometry for two different models. The orientation of the graphite layers within the fiber cross section is indicated by circles and sectors for an onion-skin (left) and a radial morphology (right), respectively. The shaded area corresponds to the regions which fulfill the Bragg condition, assuming a distribution of tilt angles of about 20° (corresponding to the azimuthal angular width of the 002 reflections in Fig. 1). The vertical lines indicate the volume illuminated by the X-ray beam with diameter D as it is scanned across the fiber. Only the intersection of the beam with the shaded areas contributes to the 002 reflection. It is obvious from this sketch that the intensity would decrease versus the center of the fiber for the onion-skin morphology, whereas it would increase versus the center of the fiber for the radial morphology.

To calculate I_{002} for these model functions, equation (1) was rewritten

$$\Omega(y) = f(y) \otimes \{M(y) d(y)\} \quad (3)$$

and Ω was calculated for both models. The results are shown in Figs. 5c and 5d together with the experimental data. It is obvious from the figure that the onion-skin model (dashed-dotted lines) can be discarded for both fibers. For *FT500* (Fig. 5d) the radial model describes the data much better than the random model. Since the fiber *HTA7* was much thinner, the data are almost resolution limited, and the curves are not very sensitive to a discrimination between the random and the radial model (Fig. 5c). However, reconsidering the results from the experiments with the beam parallel to the fiber axis, a consistent picture can finally be drawn for the two fibers investigated:

- A random arrangement of carbon layers and pores is consistent with the data for the PAN-based fiber *HTA7*. A different structure at the skin and in the core of PAN-based fibers has frequently been observed (e.g., Ruland, 1990). We could, however, not resolve such an effect in the present experiment, probably because the position resolution was not sufficient (i.e., the skin could be very thin).
- The structure of *FT500* corresponds to the radial model, i.e., the carbon layers and the (shelf-like) pores are arranged radially within the fiber cross section.

Even though the qualitative picture for the fiber geometry experiments presented in Figs. 4 and 5 is able to distinguish roughly between different structural models, it has to be further improved. For a detailed calculation of I_{002} , not only the beam profile but also the

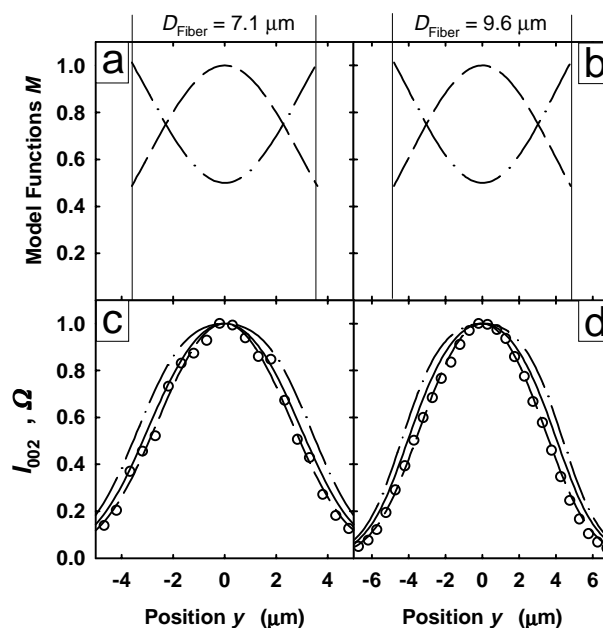


Figure 5

Model functions $M(y)$ for (a) *HTA7* and (b) *FT500* representing the increase of intensity for the radial model (dashed lines) and the decrease of intensity for the onion-skin model (dashed-dotted lines) versus the center of the fibers according to the sketch in Fig. 4. As in Fig. 2, the experimental data I_{002} are shown by the open circles for (c) *HTA7* and (d) *FT500*. The calculated distributions Ω from equation (3) are shown for the radial model (dashed lines) and for the onion-skin model (dashed-dotted lines). The full lines recall Ω for the case of $M(y) = \text{constant}$, i.e. the random model.

beam divergence has to be taken into account. Furthermore, the three-dimensional distribution of tilt angles of the carbon layers illuminated in a certain volume has to be modeled from a detailed analysis of the Bragg reflections. Finally, it has to be mentioned that the above picture assumes a constant volume fraction of carbon and pores within the fibers. The volume fraction as a function of position within the fiber cross section may be derived by calculating the integrated intensity of the SAXS signals. The detailed analysis of all reflections and the SAXS data should enable a quantitative modeling of the internal structure of the fibers from the standard fiber geometry experiments. This work is currently still in progress and will be published elsewhere.

5. Conclusions

We investigated the internal arrangement of carbon layers and pores in two different single carbon fibers using synchrotron radiation microbeam SAXS and WAXD. It could be demonstrated clearly, that this novel technique is able to discriminate between different models for the internal structure of single carbon fibers. In particular, it was possible to obtain the information also from standard fiber geometry experiments. This opens the possibility to investigate single fibers in a non-destructive way, and thus to correlate structural changes with mechanical properties by performing *in situ-tension* experiments.

Several important factors contributing to the success of the present investigation should be stressed once again:

- (i) A beam-size of only about 3 μm allowed the imaging of the nanostructure with micrometer resolution by scanning the fibers through the beam.
- (ii) Even though the size of the X-ray beam was only a factor 2 to 3 smaller than the diameter of the fibers, position-resolved information was obtained by taking the exact beam profile into account.
- (iii) Acquiring WAXD- and SAXS data with one single 2D-detector provided complementary information about the carbon layer structure and the pores simultaneously.
- (iv) Two dimensional mesh-scans using a scattering geometry with the fiber axis parallel to the beam yielded a more direct interpretation of the internal arrangement of pores and could therefore support the interpretation of the standard fiber geometry experiments.

In conclusion, the present investigation demonstrated once more the potential of X-ray microbeam scattering techniques to investigate complex, hierarchically structured materials. Important questions in materials science may be addressed in future studies, such as *in-situ* tensile tests of single carbon fibers and the investigation of the interfacial structure between fibers and matrix in carbon/carbon composites.

References

- Bennett, S. C. & Johnson, D. J. (1979). *Carbon* **17**, 25-39.
- Edie, D. D. & Stoner, E. G. (1992). *Carbon-Carbon Materials and Composites*, edited by J. D. Buckley & D. D. Edie, pp. 41-69. Park Ridge, NJ, USA: Noyes Publications.
- Fourdeux, A., Perret, R. & Ruland, W. (1968). *J. Appl. Cryst.* **1**, 252-254.
- Fratzl, P., Jakob, H. F., Rinnerthaler S., Roschger, P. and Klaushofer K. (1997). *J. Appl. Cryst.* **30**, 765-769.
- Gupta, A., Harrison, I. R. & Lahijani J. (1994). *J. Appl. Cryst.* **27**, 627-636.
- Hammersley, A. (1999). *ESRF webpage*, hyperlink: http://www.esrf.fr/computing/expg/subgroups/data_analysis/FIT2D/
- Kobets, L. P. & Deev, I. S. (1997). *Comp. Sci. Techn.* **57**, 1571-1580.
- Lichtenegger, H., Müller, M., Paris, O., Riekel, C. & Fratzl, P. (1999). To appear in *J. Appl. Cryst.* **32**.
- Müller, M., Czihak, C., Vogl, G., Fratzl, P., Schober, H. & Riekel, C. (1998). *Macromolecules* **31**, 3953-5957.
- Perret, R. & Ruland, W. (1969). *J. Appl. Cryst.* **2**, 209-218.
- Perret, R. & Ruland, W. (1970). *J. Appl. Cryst.* **3**, 525-532.
- Peterlik, H., Fratzl P. & Kromp K. (1994). *Carbon* **32**, 939-945.
- Riekel, C., Cedola, A., Heidelberg, F. & Wagner, K. (1997). *Macromolecules* **30**, 1033-1037.
- Ruland, W. & Tompa H. (1968). *Acta Cryst.* **A24**, 93-99.
- Ruland, W. (1990). *Adv. Mater.* **2**, 528-536.
- Takaku A. & Shioya M. (1990). *J. Mat. Sci.* **25**, 4873-4879.